



HAL
open science

Coalescence times, life history traits and conservation concerns: An example from four coastal shark species from the Indo-Pacific

Pierre Lesturgie, Serge Planes, Stefano Mona

► **To cite this version:**

Pierre Lesturgie, Serge Planes, Stefano Mona. Coalescence times, life history traits and conservation concerns: An example from four coastal shark species from the Indo-Pacific. *Molecular Ecology Resources*, 2021, 10.1111/1755-0998.13487 . hal-03359531

HAL Id: hal-03359531

<https://hal.sorbonne-universite.fr/hal-03359531v1>

Submitted on 30 Sep 2021

HAL is a multi-disciplinary open access archive for the deposit and dissemination of scientific research documents, whether they are published or not. The documents may come from teaching and research institutions in France or abroad, or from public or private research centers.

L'archive ouverte pluridisciplinaire **HAL**, est destinée au dépôt et à la diffusion de documents scientifiques de niveau recherche, publiés ou non, émanant des établissements d'enseignement et de recherche français ou étrangers, des laboratoires publics ou privés.

MOLECULAR ECOLOGY RESOURCES

Coalescence times, life history traits and conservation concerns: an example from four coastal shark species from the Indo-Pacific

Journal:	<i>Molecular Ecology Resources</i>
Manuscript ID	MER-21-0182.R1
Manuscript Type:	Resource Article
Date Submitted by the Author:	27-Jul-2021
Complete List of Authors:	Lesturgie, Pierre; Museum National d'Histoire Naturelle, Origines et Evolution Planes, Serge; Université de Perpignan, UMR 5244 CNRS-EPHE-UPVD; CRIOBE, UMS 2978 Mona, Stefano; Museum National d'Histoire Naturelle, Origines et Evolution; EPHE PSL
Keywords:	Coalescence, Population Genomics, Meta-Population, Sharks, Life History Traits

1 **Coalescence times, life history traits and conservation concerns: an example from four**
2 **coastal shark species from the Indo-Pacific**

3

4 Running title: Coalescence times and conservation concerns.

5

6

7 Pierre Lesturgie¹, Serge Planes^{2,4}, Stefano Mona^{1,2,3,*}

8

9 ¹ Institut de Systématique, Evolution, Biodiversité, ISYEB (UMR 7205), Muséum National
10 d'Histoire Naturelle, CNRS, Sorbonne Université, EPHE, Université des Antilles, Paris,
11 France.

12 ² EPHE, PSL Research University, Paris, France.

13 ³ Laboratoire d'Excellence CORAIL, Papetoai, French Polynesia.

14 ⁴ PSL Research University: EPHE-UPVD-CNRS, USR 3278 CRIOBE, Université de
15 Perpignan, 52 Avenue Paul Alduy, 66860, Perpignan, Cedex, France

16

17

18 * Corresponding author. E-mail : stefano.mona@mnhn.fr

19 **Abstract**

20 Dispersal abilities play a crucial role in shaping the extent of population genetic structure, with
21 more mobile species being panmictic over large geographic ranges and less mobile ones
22 organized in meta-populations exchanging migrants to different degrees. In turn, population
23 structure directly influences the coalescence pattern of the sampled lineages, but the
24 consequences on the estimated variation of the effective population size (N_e) over time obtained
25 by means of *unstructured* demographic models remain poorly understood. However, this
26 knowledge is crucial for biologically interpreting the observed N_e trajectory and further
27 devising conservation strategies in endangered species. Here we investigated the demographic
28 history of four shark species (*Carharhinus melanopterus*, *Carharhinus limbatus*, *Carharhinus*
29 *amblyrhynchos*, *Galeocerdo cuvier*) with different degrees of endangered status and life history
30 traits related to dispersal distributed in the Indo-Pacific and sampled off New Caledonia. We
31 compared several evolutionary scenarios representing both *structured* (meta-population) and
32 *unstructured* models and then inferred the N_e variation through time. By performing extensive
33 coalescent simulations, we provided a general framework relating the underlying population
34 structure and the observed N_e dynamics. On this basis, we concluded that the recent decline
35 observed in three out of the four considered species when assuming *unstructured* demographic
36 models can be explained by the presence of population structure. Furthermore, we also
37 demonstrated the limits of the inferences based on the sole site frequency spectrum and warn
38 that statistics based on linkage disequilibrium will be needed to exclude recent demographic
39 events affecting meta-populations.

40 **Introduction**

41 Reconstructing the evolutionary history of a species is a challenging exercise only partially
42 eased by the growing size of genetic data available. **Indeed**, larger amounts of data will provide
43 more precision but not more accuracy if the model(s) chosen to infer demographic parameters
44 is distant from the true one. Species are dynamic entities whose geographic range has often
45 changed in time **through** range expansions, contractions and shifts (Arenas, Ray, Currat, &
46 Excoffier, 2012; Excoffier, Foll, & Petit, 2009; Mona, Ray, Arenas, & Excoffier, 2014). **As a**
47 **consequence**, **many** species are most likely organized in meta-populations (i.e. groups of demes
48 or sub-populations exchanging migrants to some extent), even though the more vagile ones
49 might be panmictic at a large scale (Corrigan et al., 2018; Karl et al., 2010). Neglecting the
50 meta-population structure (i.e., performing demographic inferences under *unstructured*
51 models) may lead to spurious inference of population size change (Chikhi, Sousa, Luisi,
52 Goossens, & Beaumont, 2010; Maisano Delsler et al., 2019, 2016; Mazet, Rodríguez, & Chikhi,
53 2015), which is particularly worrisome for species of conservation concern. Unfortunately, the
54 link between the inferred temporal trajectory of the effective population size (N_e) and the real
55 demographic history of the meta-population remains largely under explored. However, the role
56 of connectivity, particularly the number of migrants Nm exchanged each generation and the
57 migration matrix, has been put forward as a key actor in shaping the gene genealogy of lineages
58 sampled from a deme belonging to a meta-population (Chikhi et al., 2010; Mona et al., 2014;
59 Ray, Currat, & Excoffier, 2003; Städler, Haubold, Merino, Stephan, & Pfaffelhuber, 2009).

60 Understanding the relations between meta-population structure, the inferred N_e variation under
61 *unstructured* models, and species dispersal abilities, is crucial to correctly interpret the pattern
62 of genetic variability and to establish conservation priorities. To search for general rules
63 describing such relations, we followed an inductive approach investigating species: i) with large

64 distribution (which in principle should guarantee an organization in meta-populations); ii) with
65 different life history traits (LHT) related to dispersal; iii) of conservation concerns. In this spirit,
66 we selected for our genomic study four shark species (*Carcharhinus amblyrhynchos*,
67 *Carcharhinus limbatus*, *Carcharhinus melanopterus*, and *Galeocerdo cuvier*) from New
68 Caledonia. These species have a large and overlapping distribution in the Indo-Pacific
69 (<https://sharkrays.org/>) and they differ for LHT features such as size (which is positively
70 correlated with the capacity for long distance swimming and oceanic migration (Parsons,
71 1990)), residency pattern, and long-distance dispersal ability as measured by tagging data
72 (Table S1). Moreover, the IUCN red list reported that the black-tip shark (*C. limbatus*) and the
73 tiger shark (*G. cuvier*) are Near Threatened (with a decreasing trend in the tiger shark), the
74 black-tip reef shark (*C. melanopterus*) is Vulnerable with decreasing trend, and the grey reef
75 shark (*C. amblyrhynchos*) is Endangered with decreasing trend as well. We first compared
76 several population genetics models by means of coalescent simulations coupled with an
77 approximate Bayesian computation framework (Bertorelle, Benazzo, & Mona, 2010) to detect
78 whether panmixia or a meta-population model best describe the genomic variation of each
79 species. Then, we inferred the demographic parameters under the most likely model and applied
80 the *stairwayplot*, which assumes a panmictic unstructured population (Liu & Fu, 2015), to
81 detect the N_e variation through time in each species. We finally run extensive coalescent
82 simulations under the tested meta-population models with parameters compatible to those
83 observed in real data. The simulated datasets were in turn analysed with the *stairwayplot* to: i)
84 help interpreting the observed data in the four shark species; ii) providing general coalescence
85 arguments relating the demographic history of a meta-population and the reconstructed
86 variation in N_e through time by means of *unstructured* models.

87

88 **Material & Methods**

89 **Sampling**

90 Eight specimens of tiger shark (*G. cuvier*), 13 black tip shark (*C. limbatus*), and 12 grey reef
91 shark (*C. amblyrhynchos*) were collected off New Caledonia. Total genomic DNA was
92 extracted from muscle tissue or fin clips, and preserved in 96% ethanol using QIAGEN DNeasy
93 Blood and Tissue purification kit (Qiagen, Hilden, Germany) according to the manufacturer's
94 protocols. Double-digest restriction-associated DNA (ddRAD) libraries were prepared
95 following Peterson, Weber, Kay, Fisher and Hoekstra (2012) using EcoRI and MspI restriction
96 enzymes and a 400-bp size selection. The genomic libraries obtained were sequenced with a
97 HiSeq 2500 Illumina sequencer (single-end, 125 bp). Exon capture data of eight *C.*
98 *melanopterus*) from New Caledonia (Maisano Delser et al., 2019) were included in this study
99 for comparative purposes.

100 ***De novo* assembly and data filtering (dd-RADseq samples)**

101 Raw reads were first demultiplexed and quality filtered through the *process_radtags.pl* pipeline
102 in *Stacks* v.2.5 (Rochette, Rivera-Colón, & Catchen, 2019). In the absence of a reference
103 genome for any of the three species, RAD-seq loci were *de novo* assembled independently in
104 each species under the *denovo_map.pl* pipeline in *Stacks*. We used the following assembly
105 parameters: $m=3$ (minimum read depth to create a stack), $M=4$ (number of mismatches allowed
106 between loci within individuals), and $n=4$ (number of mismatches allowed between loci within
107 catalogue). We found an average coverage per species of $\sim 10x$ (see results). A consensus on
108 the threshold below which SNP calling may be considered unreliable is still lacking. However,
109 genotype free estimation of allele frequency is generally recommended with low to medium
110 coverage (Korneliussen, Albrechtsen, & Nielsen, 2014). This approach, implemented in the
111 software *Angsd* v.0.923 (Korneliussen et al., 2014), has been rarely applied to Rad-seq data

112 (however, see Warmuth and Ellegren (2019) for an exception) and, to our knowledge, never to
113 Rad-seq data from non-model organisms, probably due to the need of a reference sequence for
114 the software to work. Here, we followed the approach of Heller et al. (2021) and Khimoun et
115 al. (2020) by creating an artificial reference sequence. First, we used the *population* script in
116 *Stacks* to *assemble* loci present in at least 80% of the individuals (using the flag $r=0.8$); then,
117 we concatenated the consensus sequences of the retrieved loci spaced by a stretch of 120 N
118 (unknown) characters (the same length of the Rad-loci) to facilitate the subsequent mapping.
119 Raw reads were then mapped back to the novel reference sequence by means of the *bwa-mem*
120 algorithm with default parameters (Li & Durbin, 2009). Using custom bash scripts coupled with
121 *Angsd*, we applied a number of filters to the aligned data and eliminated: *i*) sites with coverage
122 <3 (*-minIndDepth=3* flag), *ii*) bad quality bases and poorly aligning reads (*-minQ* and -
123 *minMapQ* and *-C* flags with default values); *iii*) poor quality sites based on the per base
124 alignment quality (*-baq=1* flag); *iv*) SNPs in the last 5 bp of each locus; *v*) SNPs heterozygote
125 in at least 80% of individuals; *vi*) loci with more than 5 SNPs that could potentially be
126 paralogous; *vii*) sites with missing data by setting the *-minInd* flag to the total number of
127 individuals retained in each species. The filtered dataset was then used to generate a site allele
128 frequency likelihood file, with the genotype likelihoods computed with the SAMtools method
129 (*-GL=1* flag), further optimised to compute a folded *site frequency spectrum* (SFS) with no
130 missing data for downstream analyses. An alternative (and simpler) approach would have been
131 to augment *m* to achieve an higher coverage (Paris, Stevens, & Catchen, 2017). However,
132 beside the considerable loss in the number of assembled loci (and hence of retrieved SNPs), we
133 found by extensive simulation of *in silico* Rad experiments that selecting high coverage loci
134 biases the SFS towards low frequency variants (Mona, Bertorelle, Benazzo, in preparation).

135 The SFS for *C. melanopterus* was estimated directly from the high coverage exon-capture
136 dataset of Maisano Delser et al. (2019).

137 **Genetic diversity and demographic inferences**

138 Nucleotide diversity (θ_π), θ_w (Watterson's theta, based on segregating sites (Watterson, 1975))
139 and Tajima's D (TD , (Tajima, 1989)) were computed from the SFS for each species with custom
140 scripts. Significance of TD was evaluated after 1,000 coalescent simulations of a constant
141 population model with scaled size θ_π . To test whether sampled demes are isolated or belong to
142 a structured meta-population and to eventually estimate connectivity, we devised three
143 alternative evolutionary models for each species (Figure 1) within an *approximate bayesian*
144 *computation* (ABC) framework. Model NS (non-structured) defined an isolated population
145 characterized by a modern effective population size (N_{MOD}) switching instantaneously into an
146 ancestral population size (N_{ANC}) at T_c generations before present. Model FIM specifies a non-
147 equilibrium finite island model defined by $d=100$ demes exchanging Nm migrants each
148 generation under a symmetric migration matrix. The array of demes is instantaneously
149 colonized T_{COL} generations before present from a population with an ancestral size (N_{ANC}).
150 Model SST is similar to FIM but demes exchange migrants only with their four neighbours (or
151 less, if they are at the border of the array), in a steppingstone fashion. We performed 50,000
152 coalescent simulations from prior distributions using *fastsimcoal* v.2.6.0.3 (Excoffier,
153 Dupanloup, Huerta-Sánchez, Sousa, & Foll, 2013), reproducing the exact number of individuals
154 and loci for each species (Table 1). We first performed model selection through the random
155 forest (RF) classification method implemented in the abcRF R package (Pudlo et al., 2016). We
156 then performed 50,000 additional simulations under the most supported model in order to
157 estimate demographic parameters with the abcRF regression method (Raynal et al., 2019). Both
158 model selection and parameter estimation were computed with the following set of summary

159 statistics: the SFS, θ_π , θ_w and TD . The first two axes of a Linear Discriminate Analysis
160 performed on the previous statistics were also included for model selection in order to increase
161 the accuracy of the estimates (Pudlo et al., 2016). Even though θ_π , θ_w and TD are function of
162 the SFS, they convey additional information by the non-linear feature of the functions.
163 Information redundancy among the considered summary statistics is accounted for by the RF
164 algorithm. Model selection and parameter estimation were run twice on each set of simulations
165 to check the consistency of the analyses, and cross validation (or confusion matrix for the model
166 selection) was performed on the first of the two runs. The number of trees in each RF algorithm
167 was chosen by monitoring the evolution of the out-of-bag error (Pudlo et al., 2016).

168 We investigated the variation in the effective population size (N_e) through time by running the
169 composite likelihood approach implemented in the *stairwayplot* v.0.2 software (Liu & Fu,
170 2015). We set the generation time to seven years for *C. melanopterus* (Maisano Delser et al.,
171 2016) and to 10 years for the other species (Cortés, 2002; Pirog et al., 2019) for all demographic
172 inferences. We applied a mutation rate per generation per site of 8.4×10^{-9} to the exon capture
173 data of *C. melanopterus* (Maisano Delser et al. 2016) and of 1.93×10^{-8} to the RADseq data for
174 the remaining three species. This mutation rate was determined by scaling genetic diversity
175 between ddRAD (obtained under the same protocol of this study) and Exon Capture data from
176 12 *C. melanopterus* individuals from Moorea, French Polynesia (Supplementary Material).

177 **Simulation study**

178 We ran coalescent simulations under FIM, SST and their modified version FIM-CH and SST-
179 CH, where the Nm parameter is changed at T_{CH} generations B.P. (Figure 1), to first inspect the
180 shape of the SFS and to further uncover the variation of N_e over time assuming a panmictic
181 population by means of the *stairwayplot*. We investigated in total 288 demographic scenarios
182 under the four meta-population models (Tables 2, S2, S3, S4, S5 and S6). Similarly to the

183 analyses performed on the real data, all scenarios were represented by $d=100$ demes exchanging
184 migrants. We sampled 10 diploid individuals either from a randomly selected deme in the case
185 of FIM/FIM-CH (since all demes have the same coalescence history) or from the central deme
186 of the array in the case of SST/SST-CH (to avoid border effects). Deme size was fixed to N_{DEME}
187 $=5000$ with m varying accordingly to obtain a long-term Nm of 1, 5, 10, and 15 in order to
188 encompass the range of the estimated values (see results). T_{COL} was fixed to 5,000, 15,000 and
189 50,000 generations B.P. or to ∞ (i.e., equilibrium model), and the ancestral effective size was
190 fixed to $N_{ANC} = 50,000$. Change of connectivity occurred at $T_{CH} = 10$ or 50 generations B.P., to
191 mimic human induced effects due to overfishing and/or habitat modifications (i.e., climate
192 changes). Looking forward in time, we modelled the change in connectivity by instantaneously
193 decreasing m or N_{DEME} by a factor 10 or 100 with respect to the long-term Nm (Tables S3, S4,
194 S5 and S6). For each combination of parameters, we performed 100 coalescent simulations of
195 50,000 Rad-like loci of 115 bp. Mutation rate per site per generations was set to 1.93×10^{-8} and
196 the generation time to 10 years. We computed for each scenario (averaged over the 100
197 replicates): a) summary statistics (θ_π , θ_w , and TD); b) the normalised SFS as in (Lapierre,
198 Lambert, & Achaz, 2017); c) the *stairwayplot*, to reconstruct the apparent variation of N_e
199 through time. We note that the number of diploid individuals and simulated loci were chosen
200 to be consistent with our data (preliminary analyses conducted on a subsample of 5,000 loci
201 produced consistent results).

202

203 **Results**

204 Summary statistics (number of assembled loci, SNPs, genetic diversity and Tajima's D) are
205 presented in Table 1. Mean coverage (and standard deviation) per sample was 9.02 (\pm 2.62),
206 7.93 (\pm 0.48), 8.39 (\pm 0.81) for *G. cuvier*, *C. limbatus* and *C. amblyrhynchos* respectively.

207 We compared the models NS, FIM, and SST (Figure 1) in the four species by means of an
208 ABC-RF algorithm and estimated demographic parameters for the most supported model. After
209 checking for the evolution of the out-of-bag error of the RF, model selection and parameter
210 estimation were computed using respectively 500 and 1,000 trees in each species. We found
211 that NS had the higher posterior probability ($p=0.84$) for *G. cuvier* (Tables 1 and S7). In
212 contrast, demographic histories of the three other species were best described by SST, with a
213 posterior probability ranging from 0.53 to 0.88 (Tables 1 and S7). The estimated median
214 number of migrants per generation Nm was 1.8 (95% CI: 0.7-3.0) for *C. melanopterus*, 6.6 (95%
215 CI: 1.5-15.4) for *C. limbatus*, and 11.5 (95% CI: 3.0-22.0) for *C. amblyrhynchos* (Figure 2,
216 Table 1). The posterior distribution of Nm strongly differed from the prior distribution and
217 showed a clear unimodal peak with small credible intervals, and low mean square error (SME)
218 and mean root square error (SMRE) in all three species (Figure 2, Table S8, suggesting that
219 these estimates are highly reliable. Conversely, both T_{COL} and N_{ANC} had larger SME and SMRE
220 errors in all species (Table S8), but it was only in *C. melanopterus* where posterior and prior
221 distribution could not be distinguished (Figure 2). T_{COL} has a clear unimodal distribution in *C.*
222 *amblyrhynchos* but a more disperse one (and with wider credible intervals) in *C. limbatus*
223 (Figure 2, Table 1).

224 The *stairwayplot* showed a nearly similar dynamic for *C. amblyrhynchos* and *C. limbatus*,
225 characterized by a strong ancestral expansion (Figure 3). When approaching $T=0$, both species
226 underwent a bottleneck but of distinct strength. This is consistent with the shape of the
227 normalized SFS, which clearly shows a stronger deficit in low frequency variants for *C.*
228 *limbatus* compared to *C. amblyrhynchos* (Figure 3). Similarly to *C. limbatus*, *C. melanopterus*
229 experienced a recent 10-fold population collapse around 20,000 years B.P. starting from a long
230 term constant N_e . However, *C. melanopterus* showed no signature of ancestral expansion,

231 consistent to the results obtained by Maisano Delser et al. (2019) using *abc-skyline* method.
232 Finally, *G. cuvier* displayed an ancestral expansion around 100,000 years B.P. with N_e reaching
233 $\sim 12,000$ before dropping to ~ 3000 at $T \sim 1,600$ years B.P. Remarkably, the ancestral expansion
234 retrieved by the *stairwayplot* (Figure 3) for both *C. amblyrhynchos* and *C. limbatus* overlap
235 with the posterior distribution of T_{COL} estimated by the SST model (Table 1). This analogy
236 holds too for *C. melanopterus*, where T_{COL} could not be properly estimated under the structured
237 model (we obtained a flat posterior distribution, Figure 2) and there was no signature of
238 ancestral expansion in the *stairwayplot* (Figure 3).

239 The first set of coalescent simulations was run under FIM and SST only (Table 2 and S2 to
240 check if simulated data could reproduce the pattern of genetic variability (both θ estimators and
241 TD) observed for *C. melanopterus*, *C. limbatus*, and *C. amblyrhynchos*. The simulated θ values
242 (excluding the equilibrium model) ranged between 0.001 and 0.003 per site, in line with the
243 observed values (Table 1 and 2). TD follows a U-shaped distribution for each Nm value as a
244 function of T_{COL} , being more positive at recent T_{COL} and at equilibrium and less positive (or
245 negative for higher Nm) at intermediate values. Therefore, species demography with $Nm \sim 10$
246 (and higher) and T_{COL} within 15k and 50k generations B.P. will have negative TD values. In
247 contrast, species with lower Nm and very recent or very ancient T_{COL} will have positive TD .
248 This matches strikingly the TD observed for the three shark species and their estimated
249 demographic parameters under SST (Table 1). We plot the normalized SFS and the *stairwayplot*
250 for all scenarios presented in Table 2 (Figures 4, 5, S1, S2 and S3). First, we note that none of
251 our scenarios, even those at equilibrium and with no variation in Nm through time, showed a
252 normalized SFS compatible with a constant size population (Figures 4, 5, S1, S2 and S3). The
253 normalized SFS and the reconstructed *stairwayplot* depend generally on the interaction between
254 Nm and T_{COL} with a dynamic strikingly similar to TD (which is indeed a summary of the SFS).

255 For $Nm=1$ we observed the signature of a recent decrease in N_e for all scenarios and
256 independently of T_{COL} (Figure 4). The normalized SFS showed consistently a strong deficit of
257 low frequency variants, typical of a demographic bottleneck and in agreement with the positive
258 TD (Figure 4 and Table 1). Furthermore, the *stairwayplot* could never detect the ancestral
259 expansion for any T_{COL} . For growing Nm , the interplay with T_{COL} becomes more complex. A
260 general result is that, once again, all scenarios were characterized by a recent decrease of N_e
261 when looking at the *stairwayplot* and a deficit of singletons compared to the other low
262 frequency classes when looking at the normalized SFS (Figures 5, S1 and S2). However, a
263 strong signature of ancestral expansion appeared for $Nm > 10$ and T_{COL} between 15k and 50k
264 generations B.P., mirroring the results of TD for which most of these scenarios displayed a
265 negative value. Remarkably, the *stairwayplot* retrieved the ancestral expansion only slightly
266 overestimating the simulated T_{COL} (Figures 5, S1 and S2). Similar results were obtained for
267 FIM (Figures S4 and S5).

268 We compared SST vs SST-CH model (Figure 1) by means of the same ABC-RF model
269 selection framework previously adopted. The two models cannot be clearly distinguished in
270 any of the three structured species since: *i*) they showed similar posterior probability (~ 0.50);
271 *ii*) the prior error rates are large ~ 0.40 (Table S9); *iii*) posterior distributions of Nm before and
272 after T_{CH} are wide and largely overlapping (Table S10); *iv*) the normalized SFS closest to the
273 observed data retrieved under the two models are very similar (Figure S6). We ran a second set
274 of coalescent simulations focusing on the consequences of a recent change in connectivity on
275 the observed SFS and the reconstructed *stairwayplot* (Table S3 and S4). The decrease in
276 connectivity was simulated by reducing either m (the migration rate per generation) or N_{DEME}
277 (the effective population size of each deme). As expected, we found a signature of recent
278 population decline in all simulated scenarios, with its intensity only slightly affected by the

279 change in Nm (Figures 6, S7, S8 and S9). However, the drop in N_{DEME} (Figures 6 and S9) had
280 larger effect compared to the drop in m (Figures S7 and S8) on both the normalized SFS and
281 the expansion time estimated by the *stairwayplot*. In scenarios with 100x reduction in N_{DEME} ,
282 the *stairwayplot* could not retrieve the ancestral expansion even for large long-term Nm (Figure
283 6). FIM-CH models displayed a behaviour similar to SST-CH models but more pronounced
284 (Figures S10, S11, S12 and S13, Table S5 and S6). While at $T_{CH} = 10$ a decrease in Nm slightly
285 affected the SFS and the reconstructed *stairwayplot*, the consequence of the change in
286 connectivity are more substantial at $T_{CH} = 50$, with a stronger deficit in singletons and a more
287 pronounced recent decline in N_e particularly in scenarios with a 100-fold reduction of N_{DEME}
288 (Figures S11 and S13).

289

290 Discussion

291 *Life history traits and demographic history of the four shark species*

292 Discriminating whether the most appropriate model to reconstruct the demographic history of
293 a species is *structured* or *unstructured* should be the first step in empirical population genetics
294 investigations, particularly when targeting species of conservation concerns. Even when an
295 extensive spatial sampling is lacking, an ABC model selection approach can actually
296 distinguish whether the sampled deme belongs or not to a meta-population (similarly to
297 previous studies (Maisano Delser et al., 2019; Peter, Wegmann, & Excoffier, 2010)). **Among**
298 **the four species considered here, the tiger shark is the only panmictic. The three other species**
299 **conversely are best described by the SST model, i.e., the sampled populations belong to a meta-**
300 **population exchanging migrants following a stepping stone matrix. Our results reflect the tight**
301 **link between the level of meta-population structure (or its absence) and life history traits. The**

302 panmictic *G. cuvier* unsurprisingly can accomplish transoceanic movements and has the largest
303 body size among the sharks here considered (Table S1). In the three other species, the estimated
304 number of migrants (Nm) remarkably follows the increase of movement range (Table 1 and S1)
305 and it is consistent with their behaviour and habitat use. Indeed, *C. melanopterus*, a strongly
306 lagoon dependent species, displays the lowest level of connectivity among the studied species
307 (Tables 1 and S1). These results bring meaningful hints about the influence of life history traits
308 on population structure in sharks, but more studies addressing this topic will be needed to
309 accurately detect which traits best predict its extent.

310 ***Gene genealogies in the four shark species and simulated scenarios***

311 While it may seem counterintuitive to apply *unstructured* models to demes belonging to a meta-
312 population, we further investigated the demographic history of the four species by means of the
313 *stairwayplot*. When enough data is available, non-parametric *unstructured* models (such as the
314 PSMC (Li & Durbin, 2011), the extended Bayesian skyline plot (Heled & Drummond, 2008)
315 and the *stairwayplot* among others) provide a careful description of the distribution of
316 coalescence times of the gene genealogy, which ultimately depends from the “true”
317 demographic history (whether it is known or not) of the sampled lineages. If panmixia is the
318 most likely scenario, the distribution of coalescence times is directly related to the variation of
319 N_e through time and can therefore have a direct biological interpretation. This is the case for *G.*
320 *cuvier* (Table 1), whose reconstructed *stairwayplot* suggests that this species experienced a mild
321 ancestral expansion and a recent ~4-fold bottleneck around 2,000 years B.P. (consistent with
322 the results of Pirog et al. (2019), Figure 3). Conversely, signals detected by the *stairwayplot* in
323 the remaining three species, better described by the SST model (Table 1), cannot be directly
324 interpreted as changes in N_e over time. In this light, we ran coalescence simulations to provide

325 helpful and general insights into the understanding of the relation between the inferences
326 performed under *unstructured* and *structured* models.

327 We first focus on scenarios simulated under the SST, with parameters close to those estimated
328 in real data. The first and most striking result is that we systematically observed a recent
329 bottleneck under all simulated scenarios (Table 2, Figures 4, 5, S1, S2 and S3). This result could
330 seem at a first glance surprising and due to an artefact. However, this is not the case, as: i) the
331 signal does not depend on the inferential algorithm chosen to analyse the data (i.e., the
332 *stairwayplot*), since the normalized spectra showed a deficit in singletons compared to the other
333 low frequency classes (Figures 4, 5, S1 and S2), which is typical of a recent population decline;
334 ii) it is consistent with the distribution of the Inverse Instantaneous Coalescence Rate (IICR)
335 computed in one diploid individual, which shows a signature of decline under similar meta-
336 population models (Chikhi et al., 2018; Mazet, Rodríguez, Grusea, Boitard, & Chikhi, 2016;
337 Rodríguez et al., 2018). The results of our simulations are consistent with the recent bottleneck
338 observed in the three shark species (Figure 3), with its intensity inversely correlated to the
339 estimated Nm (i.e., stronger for *C. melanopterus* and *C. limbatus* than for *C. amblyrhynchos*).

340 In our SST model there is an instantaneous colonization of the array of demes at T_{COL} , which
341 corresponds also to a demographic expansion (i.e., the total number of individuals in the array
342 of deme is larger than those in the ancestral deme). However, this signature is detected only for
343 $Nm \geq 5$ when T_{COL} is neither too recent nor too old (at equilibrium) (Figures 5, S1, S2 and S3).

344 In these scenarios, the beginning of the expansion retrieved by the *stairwayplot* broadly
345 corresponds to the simulated T_{COL} . This again corroborates the results obtained for the three
346 shark species, since the two species with higher Nm displayed indeed an ancestral expansion in
347 the *stairwayplot* with a timing consistent with the estimated T_{COL} (Table 1, Figures 2 and 3).

348 Similarly, it explains why we could not retrieve the ancestral expansion for *C. melanopterus*

349 nor estimate T_{COL} under the SST model: this appears to be a property of the coalescence pattern
350 and it is not related to the amount of data available (see below).

351 *Coalescence phases in structured models*

352 It is now straightforward to frame all these findings under the coalescence perspective. The
353 coalescence history of the lineages sampled from a single deme in an SST (or FIM) model can
354 be separated for simplicity into three phases: the *scattering*, the *collecting* and the *ancestral*
355 phase (Figure 7). Going backward in time, lineages will coalesce in the sampled deme with a
356 rate according to both Nm and N_{DEME} until all lineages either have coalesced or migrated to
357 another deme. This is the *scattering* phase described in the seminal works of (Wakeley, 1998,
358 1999). The *scattering* phase was considered instantaneous for mathematical tractability, with
359 its outcome dependent on Nm only, but later works could disentangle the effect of N_{DEME} and
360 m on the shape of the gene genealogy (Mona, 2017). The *collecting* phase starts when the
361 lineages which did not coalesce have migrated to other demes of the array: they will then
362 coalesce according to a Kingman process with a rate scaled by Nm and the number of demes d
363 of the array (Wakeley, 1999) (Figure 7). Finally, all surviving lineages (in non-equilibrium
364 model) will reach the ancestral deme at T_{COL} , where they will coalesce at a rate depending only
365 on the N_{ANC} parameter (Figure 7). The interplay between the demographic parameters (N_{DEME} ,
366 Nm , N_{ANC} , d) and the historical events (T_{COL} and T_{CH}) determines the length of each coalescence
367 phase and the resulting shape of the gene genealogy of the sampled lineages (Figure 7).

368 In species with low Nm , the rate of coalescence during the *scattering* phase is very fast since
369 lineages have low probability of emigrating from the sampled deme and high probability of
370 coalescence due to the small N . Once all the lineages are dispersed in the array of demes, there
371 will be two possible outcomes: i) in equilibrium model, we shift to the *collecting* phase, where
372 the rate of coalescence drops since lineages will hardly fall in the same deme again; ii) in non-

373 equilibrium model, with the parameters we have simulated here, there will be very few (if any)
374 coalescence events during the collecting phase and the transition will be directly from the
375 scattering to the ancestral phase. Both the collecting and the ancestral phases have a rate of
376 coalescence lower than the scattering phase, which determines the observed recent drop in N_e
377 for all simulated scenarios. Remarkably, the decline in N_e is much stronger in equilibrium
378 model, since the rate of coalescence is much lower in the collecting than in the ancestral phase
379 (Figures 4, 5, S1, S2 and S3). Low Nm species will therefore have only two coalescence phases,
380 the scattering and either the collecting (in equilibrium model) or the ancestral (in non-
381 equilibrium model) which is why the signature of the ancestral expansion is lost.

382 For growing Nm , in equilibrium model there will be again only two coalescence phases, namely
383 the scattering and collecting, with the latter having a lower rate of coalescence than the former
384 independently of the simulated parameters. This is why we observed always a strong bottleneck
385 consistent with the distribution of the IICR statistics in any equilibrium model (Chikhi et al.,
386 2018; Mazet et al., 2015; Rodríguez et al., 2018). In non-equilibrium model, there will be two
387 different situations: a) T_{COL} (in generations) is of the same order of the deme size N_{DEME} . In this
388 setting, going backward in time few lineages would have escaped the sampled demes before
389 T_{COL} . This corresponds to a shift in the coalescence rate directly from the scattering to the
390 ancestral phase, resulting in a bottleneck of lower intensity compared to an equilibrium model
391 (Figures 4, 5, S1 and S2), for the same reasons as above; b) T_{COL} (in generations) is larger than
392 N_{DEME} . In this setting, some coalescence events may occur during the collecting phase, at a rate
393 much slower than the two other phases. This determines the hump observed in the stairwayplot
394 (Figures 4, 5, S1 and S2) and explains why in this window of parameters it is also possible to
395 correctly estimate T_{COL} using our ABC framework. Further simulations under the FIM model
396 confirmed those patterns even though the ancestral expansion could be detected for lower long-

397 term Nm than the corresponding SST scenario (Figure S4). This is probably due to a higher
398 apparent connectivity underlined the by FIM, where lineages can move more freely during the
399 collecting phase in comparison to SST where migrants only come from the closest neighbours.
400 If many coalescence events occur during the *collecting* phase, the change in coalescence rate
401 will affect the resulting gene genealogy and it will be detected by the *stairwayplot* (or any other
402 *unstructured* method based on coalescent theory).

403 *Changes in connectivity*

404 Using coalescence arguments, we clarified why simple meta-population models with constant
405 connectivity generate a gene genealogy harbouring a signature of a recent decline for any
406 parameters' combination. The signature of bottleneck detected by the *stairwayplot* in the three
407 shark species best described by SST can be therefore interpreted as a consequence of the
408 underlying structure. However, connectivity likely changes through time. For instance, human
409 activities have likely impacted the evolutionary history of a large number of species either by
410 decreasing their effective population size and/or by fragmenting their habitat (i.e., reducing
411 migration rates between demes). This intuitively should exacerbate the signature of population
412 decline in the resulting gene genealogy. However, it remains to be shown whether this signature
413 is qualitatively and quantitatively distinguishable from models with constant connectivity. This
414 is a question of fundamental importance to understand whether it is possible to detect recent
415 bottleneck in structured populations. To this end, we further investigated by coalescent
416 simulations the expected gene genealogy in SST-CH (and FIM-CH) models with a change in
417 connectivity 10 or 50 generations B.P., which matches the beginning of extensive
418 anthropogenic influence on biodiversity considering our species' generation time (Ceballos et
419 al., 2015). The resulting gene genealogies were poorly affected by the recent drop in
420 connectivity, with both the normalized SFS and the inferred N_e dynamic following the same

421 trajectory of the corresponding scenario with the same long-term Nm and T_{COL} (Figures 6, S7,
422 S8, S9, S10, S11, S12 and S13). We noticed the drop in N_{DEME} (Figures 6, S9, S12 and S13)
423 had stronger influence than the drop in m (Figures S7, S8, S10 and S11), consistent with
424 previous finding showing that the distribution of coalescence events depends not only by the
425 Nm compound parameter but also by their individuals values (Mona, 2017). This can be
426 explained once again in the light of the length of the coalescence phases (Figure 7). Reducing
427 N_{DEME} will increase exponentially the number of coalescence events, drastically shortening the
428 scattering phase and the number of surviving lineages. Reducing m will only linearly reduce
429 the probability of migrations outside the deme, marginally affecting the length of the scattering
430 phase and the number of surviving lineages compared to constant Nm scenarios. This is why a
431 100-fold reduction in N_{DEME} significantly reduces the number of lineages entering in the
432 collecting phase, almost hiding the ancestral expansion in high long-term Nm scenarios (Figures
433 6, S9, S12 and S13), while a 100-fold reduction in m is barely detectable (Figures S7, S8, S10
434 and S11). Similarly, the recent reduction in either N_{DEME} or m cannot be detected for lower
435 long-term Nm scenarios, where the collecting phase is already missing. This explains why the
436 general pattern is strikingly similar between SST-CH and SST simulations, which implies that
437 the simulated change in connectivity is too recent to significantly alter the pattern of
438 coalescence events and that a recent drop can be hardly detected on the basis of the SFS only.
439 Our empirical data are consistent with these findings: when we compared SST vs. SST-CH
440 models in the three shark species using the ABC framework, we failed to clearly distinguish
441 the two models (Tables S9 and S10, Figure S6). This seems to be a paradox: we observed a
442 recent bottleneck in species of conservation concern using *unstructured* model, but we cannot
443 exclude that this is just the consequence of population structure.

444 ***Practical recommendations and conservation concerns***

445 This study highlight once more the importance to explicitly test for meta-population structure
446 before interpreting the demographic signals detected by *unstructured* models, similarly to what
447 advocated previously by (Maisano Delsler et al., 2019; Rodríguez et al., 2018). If the meta-
448 population structure hypothesis is rejected, the variation of N_e through time can be directly
449 interpreted as the demographic history of the population under investigation, such as the case
450 of tiger shark. Otherwise, this variation is still related to demographic events, but it has to be
451 explained in the light of population structure and its consequence on the rate of coalescence
452 events. We showed by coalescent simulations how to interpret such variation: the recent
453 bottleneck detected by the *stairwayplot* in demes belonging to a meta-population is a
454 consequence of the coalescence process. In other words, any inferential method implementing
455 an *unstructured* model will detect such decline (if enough data is available) since it is a property
456 of the gene genealogy. Importantly, the gene genealogy is only slightly affected by recent
457 changes in connectivity if the time of this change in generations is of the same order of the size
458 of the deme.

459 Our study underscore a key issue in conservation genetics as a recent decline inferred by an
460 *unstructured* model can be mis-interpreted as a consequence of recent anthropic pressures
461 (Ceballos et al., 2015) when it actually results from meta-population structure. This is all the
462 more alarming since the majority of species is likely organised in meta-populations across their
463 range rather than panmictic at a large scale. We therefore stress the necessity for an educated
464 choice of tools to correctly uncover the recent trend of a species and design proper conservation
465 programs. For instance, detecting a recent bottleneck in meta-populations will require summary
466 statistics measuring the linkage disequilibrium (Boitard, Rodríguez, Jay, Mona, & Austerlitz,
467 2016; Kerdoncuff, Lambert, & Achaz, 2020) and/or the inferential framework based on the
468 IICR (Chikhi et al., 2018; Rodríguez et al., 2018) coupled with whole genome data. On a

469 positive note, we showed that the colonization time of the array of demes can be estimated to
470 some extent (and under some combinations of parameters) by *unstructured* models. We believe
471 that this is particularly important because it has been shown that the simple instantaneous
472 colonization process we used here behaves similarly to a spatial explicit range expansion
473 (Hamilton, Stoneking, & Excoffier, 2005; Mona, 2017), which is certainly a more realistic
474 model but more difficult to investigate. We are aware that the meta-population models here
475 tested are simple and the parameters chosen are specific of the three shark species we focused
476 on. Nevertheless, the time-scale separation of the coalescence process is general, and it allows
477 explaining intuitively any structured models. The four shark species here used as an example
478 has the merit to cover a large spectrum of LHT and consequently a large spectrum of
479 demographic scenarios, going from a highly structured to a panmictic population: this has
480 strong implications on the distribution of coalescence times and therefore on the interpretation
481 of the observed data.

482 *Conclusion*

483 In this study we found that population structure, independently from the degree of connectivity
484 between demes and the migration matrix relating them, intrinsically determines a variation in
485 the rate of coalescence events through time. We showed that the intensity and the direction(s)
486 of such variation related to the demographic parameters of the meta-population in a predictable
487 way. Our results highlight the importance of detecting population structure (which depends on
488 LHT among other factors) before performing any demographic inferences but, at the same time,
489 they reveal the utility of *unstructured* models to describe the shape of the gene genealogy, which
490 is the final product of the evolutionary history of a species. A combination of structured and
491 *unstructured* models (better if non-parametric) is therefore the key to best characterize the
492 evolutionary history of a species. We call for a change in perspective when investigating the

493 demographic history of a species: the focus should be put in the reconstruction of the variation
494 of both N and m through time, which requires certainly new methodological development and
495 probably more data.

496

497 **Acknowledgement**

498 We are grateful to the Genotoul bioinformatics platform Toulouse Midi-Pyrenees (Bioinfo
499 Genotoul; <http://bioinfo.genotoul.fr/>) for providing computing resources. We are indebted to
500 Oscar Lao for fruitful discussions and careful reading of the manuscript. This work was
501 supported by two ATM grants (2016 and 2017) from the Muséum National d'Histoire Naturelle
502 to S.M.

503

504 **References**

505

- 506 Arenas, M., Ray, N., Currat, M., & Excoffier, L. (2012). Consequences of range contractions
507 and range shifts on molecular diversity. *Molecular Biology and Evolution*, *29*(1), 207–
508 218. <https://doi.org/10.1093/molbev/msr187>
- 509 Bertorelle, G., Benazzo, A., & Mona, S. (2010). ABC as a flexible framework to estimate
510 demography over space and time: Some cons, many pros. *Molecular Ecology*, *19*(13),
511 2609–2625. <https://doi.org/10.1111/j.1365-294X.2010.04690.x>
- 512 Boitard, S., Rodríguez, W., Jay, F., Mona, S., & Austerlitz, F. (2016). Inferring Population
513 Size History from Large Samples of Genome-Wide Molecular Data - An Approximate
514 Bayesian Computation Approach. *PLoS Genetics*, *12*(3), e1005877.
515 <https://doi.org/10.1371/journal.pgen.1005877>
- 516 Ceballos, G., Ehrlich, P. R., Barnosky, A. D., García, A., Pringle, R. M., & Palmer, T. M.
517 (2015). Accelerated modern human-induced species losses: Entering the sixth mass
518 extinction. *Science Advances*, *1*(5), 9–13. <https://doi.org/10.1126/sciadv.1400253>
- 519 Chikhi, L., Rodríguez, W., Grusea, S., Santos, P., Boitard, S., & Mazet, O. (2018). The IICR
520 (inverse instantaneous coalescence rate) as a summary of genomic diversity: Insights
521 into demographic inference and model choice. *Heredity*, *120*(1), 13–24.
522 <https://doi.org/10.1038/s41437-017-0005-6>
- 523 Chikhi, L., Sousa, V. C., Luisi, P., Goossens, B., & Beaumont, M. A. (2010). The
524 Confounding Effects of Population Structure, Genetic Diversity and the Sampling
525 Scheme on the Detection and Quantification of Population Size Changes. *Genetics*,
526 *186*(3), 983–995. <https://doi.org/10.1534/genetics.110.118661>
- 527 Corrigan, S., Lowther, A. D., Beheregaray, L. B., Bruce, B. D., Cliff, G., Duffy, C. A., ...

- 528 Rogers, P. J. (2018). Population Connectivity of the Highly Migratory Shortfin Mako
529 (*Isurus oxyrinchus* Rafinesque 1810) and Implications for Management in the Southern
530 Hemisphere. *Frontiers in Ecology and Evolution*, 6(NOV), 1–15.
531 <https://doi.org/10.3389/fevo.2018.00187>
- 532 Cortés, E. (2002). Incorporating uncertainty into demographic modeling: Application to shark
533 populations and their conservation. *Conservation Biology*, 16(4), 1048–1062.
534 <https://doi.org/10.1046/j.1523-1739.2002.00423.x>
- 535 Excoffier, L., Dupanloup, I., Huerta-Sánchez, E., Sousa, V. C., & Foll, M. (2013). Robust
536 Demographic Inference from Genomic and SNP Data. *PLoS Genetics*, 9(10), e1003905.
537 <https://doi.org/10.1371/journal.pgen.1003905>
- 538 Excoffier, L., Foll, M., & Petit, R. J. (2009). Genetic Consequences of Range Expansions.
539 *Annual Review of Ecology, Evolution, and Systematics*, 40(1), 481–501.
540 <https://doi.org/10.1146/annurev.ecolsys.39.110707.173414>
- 541 Hamilton, G., Stoneking, M., & Excoffier, L. (2005). Molecular analysis reveals tighter social
542 regulation of immigration in patrilocal populations than in matrilocal populations.
543 *Proceedings of the National Academy of Sciences of the United States of America*,
544 102(21), 7476–7480. <https://doi.org/10.1073/pnas.0409253102>
- 545 Heled, J., & Drummond, A. J. (2008). Bayesian inference of population size history from
546 multiple loci. *BMC Evolutionary Biology*, 8(1), 289. [https://doi.org/10.1186/1471-2148-](https://doi.org/10.1186/1471-2148-8-289)
547 8-289
- 548 Heller, R., Nursyifa, C., Garcia-Erill, G., Salmona, J., Chikhi, L., Meisner, J., ... Albrechtsen,
549 A. (2021). A reference-free approach to analyse RADseq data using standard next
550 generation sequencing toolkits. *Molecular Ecology Resources*, 21(4), 1085–1097.
551 <https://doi.org/10.1111/1755-0998.13324>
- 552 Karl, S. A., Motta, P. J., Stewart, B. S., Wilson, S. G., Bowen, B. W., Castro, A. L. F., ...
553 Hueter, R. E. (2010). Population genetic structure of Earth's largest fish, the whale shark
554 (*Rhincodon typus*). *Molecular Ecology*, 16(24), 5183–5192.
555 <https://doi.org/10.1111/j.1365-294x.2007.03597.x>
- 556 Kerdoncuff, E., Lambert, A., & Achaz, G. (2020). Testing for population decline using
557 maximal linkage disequilibrium blocks. *Theoretical Population Biology*, 134, 171–181.
558 <https://doi.org/10.1016/j.tpb.2020.03.004>
- 559 Khimoun, A., Doums, C., Molet, M., Kaufmann, B., Peronnet, R., Eyer, P. A., & Mona, S.
560 (2020). Urbanization without isolation: The absence of genetic structure among cities
561 and forests in the tiny acorn ant *Temnothorax nylanderi*. *Biology Letters*, 16(1).
562 <https://doi.org/10.1098/rsbl.2019.0741>
- 563 Korneliussen, T. S., Albrechtsen, A., & Nielsen, R. (2014). ANGSD: Analysis of Next
564 Generation Sequencing Data. *BMC Bioinformatics*, 15(1), 1–13.
565 <https://doi.org/10.1186/s12859-014-0356-4>
- 566 Lapierre, M., Lambert, A., & Achaz, G. (2017). Accuracy of Demographic Inferences from
567 the Site Frequency Spectrum: The Case of the Yoruba Population. *Genetics*, 206(1),
568 439–449. <https://doi.org/10.1534/genetics.116.192708>
- 569 Li, H., & Durbin, R. (2009). Fast and accurate short read alignment with Burrows-Wheeler
570 transform. *Bioinformatics*, 25(14), 1754–1760.
571 <https://doi.org/10.1093/bioinformatics/btp324>
- 572 Li, H., & Durbin, R. (2011). Inference of human population history from individual whole-
573 genome sequences. *Nature*, 475(7357), 493–496. <https://doi.org/10.1038/nature10231>
- 574 Liu, X., & Fu, Y.-X. (2015). Exploring population size changes using SNP frequency spectra.
575 *Nature Genetics*, 47(5), 555–559. <https://doi.org/10.1038/ng.3254>

- 576 Maisano Delsler, P., Corrigan, S., Duckett, D., Suwalski, A., Veuille, M., Planes, S., ... Mona,
577 S. (2019). Demographic inferences after a range expansion can be biased: the test case of
578 the blacktip reef shark (*Carcharhinus melanopterus*). *Heredity*, 122(6), 759–769.
579 <https://doi.org/10.1038/s41437-018-0164-0>
- 580 Maisano Delsler, P., Corrigan, S., Hale, M., Li, C., Veuille, M., Planes, S., ... Mona, S.
581 (2016). Population genomics of *C. melanopterus* using target gene capture data:
582 Demographic inferences and conservation perspectives. *Scientific Reports*, 6(April), 1–
583 12. <https://doi.org/10.1038/srep33753>
- 584 Mazet, O., Rodríguez, W., Grusea, S., Boitard, S., & Chikhi, L. (2016). On the importance of
585 being structured: instantaneous coalescence rates and human evolution—lessons for
586 ancestral population size inference? *Heredity*, 116(4), 362–371.
587 <https://doi.org/10.1038/hdy.2015.104>
- 588 Mazet, Olivier, Rodríguez, W., & Chikhi, L. (2015). Demographic inference using genetic
589 data from a single individual: Separating population size variation from population
590 structure. *Theoretical Population Biology*, 104, 46–58.
591 <https://doi.org/10.1016/j.tpb.2015.06.003>
- 592 Mona, S. (2017). On the role played by the carrying capacity and the ancestral population size
593 during a range expansion. *Heredity*, 118(2), 143–153.
594 <https://doi.org/10.1038/hdy.2016.73>
- 595 Mona, S., Ray, N., Arenas, M., & Excoffier, L. (2014). Genetic consequences of habitat
596 fragmentation during a range expansion. *Heredity*, 112(3), 291–299.
597 <https://doi.org/10.1038/hdy.2013.105>
- 598 Paris, J. R., Stevens, J. R., & Catchen, J. M. (2017). Lost in parameter space: a road map for
599 stacks. *Methods in Ecology and Evolution*, 8(10), 1360–1373.
600 <https://doi.org/10.1111/2041-210X.12775>
- 601 Parsons, G. R. (1990). Metabolism and swimming efficiency of the bonnethead shark *Sphyrna*
602 *tiburo*. *Marine Biology*, 104(3), 363–367. <https://doi.org/10.1007/BF01314338>
- 603 Peter, B. M., Wegmann, D., & Excoffier, L. (2010). Distinguishing between population
604 bottleneck and population subdivision by a Bayesian model choice procedure. *Molecular*
605 *Ecology*, 19(21), 4648–4660. <https://doi.org/10.1111/j.1365-294X.2010.04783.x>
- 606 Peterson, B. K., Weber, J. N., Kay, E. H., Fisher, H. S., & Hoekstra, H. E. (2012). Double
607 Digest RADseq: An Inexpensive Method for De Novo SNP Discovery and Genotyping
608 in Model and Non-Model Species. *PLoS ONE*, 7(5), e37135.
609 <https://doi.org/10.1371/journal.pone.0037135>
- 610 Pirog, A., Jaquemet, S., Ravigné, V., Cliff, G., Clua, E., Holmes, B. J., ... Magalon, H.
611 (2019). Genetic population structure and demography of an apex predator, the tiger shark
612 *Galeocerdo cuvier*. *Ecology and Evolution*, 9(10), 5551–5571.
613 <https://doi.org/10.1002/ece3.5111>
- 614 Pudlo, P., Marin, J.-M. M., Estoup, A., Cornuet, J.-M. M., Gautier, M., & Robert, C. P.
615 (2016). Reliable ABC model choice via random forests. *Bioinformatics*, 32(6), 859–866.
616 <https://doi.org/10.1093/bioinformatics/btv684>
- 617 Ray, N., Currat, M., & Excoffier, L. (2003). Intra-deme molecular diversity in spatially
618 expanding populations. *Molecular Biology and Evolution*, 20(1), 76–86.
619 <https://doi.org/10.1093/molbev/msg009>
- 620 Raynal, L., Marin, J. M., Pudlo, P., Ribatet, M., Robert, C. P., & Estoup, A. (2019). ABC
621 random forests for Bayesian parameter inference. *Bioinformatics*, 35(10), 1720–1728.
622 <https://doi.org/10.1093/bioinformatics/bty867>
- 623 Rochette, N. C., Rivera-Colón, A. G., & Catchen, J. M. (2019). Stacks 2: Analytical methods

- 624 for paired-end sequencing improve RADseq-based population genomics. *Molecular*
625 *Ecology*, 28(21), 4737–4754. <https://doi.org/10.1111/mec.15253>
- 626 Rodríguez, W., Mazet, O., Grusea, S., Arredondo, A., Corujo, J. M., Boitard, S., & Chikhi, L.
627 (2018). The IICR and the non-stationary structured coalescent: towards demographic
628 inference with arbitrary changes in population structure. *Heredity*, 121(6), 663–678.
629 <https://doi.org/10.1038/s41437-018-0148-0>
- 630 Städler, T., Haubold, B., Merino, C., Stephan, W., & Pfaffelhuber, P. (2009). The impact of
631 sampling schemes on the site frequency spectrum in nonequilibrium subdivided
632 populations. *Genetics*, 182(1), 205–216. <https://doi.org/10.1534/genetics.108.094904>
- 633 Tajima, F. (1989). Statistical method for testing the neutral mutation hypothesis by DNA
634 polymorphism. *Genetics*, 123(3), 585–595. <https://doi.org/10.1093/genetics/123.3.585>
- 635 Wakeley, J. (1998). Segregating Sites in Wright’s Island Model. *Theoretical Population*
636 *Biology*, 53, 166–174.
- 637 Wakeley, J. (1999). Nonequilibrium migration in human history. *Genetics*, 153(4), 1863–
638 1871.
- 639 Warmuth, V. M., & Ellegren, H. (2019). Genotype-free estimation of allele frequencies
640 reduces bias and improves demographic inference from RADSeq data. *Molecular*
641 *Ecology Resources*, 19(3), 586–596. <https://doi.org/10.1111/1755-0998.12990>
- 642 Watterson, G. A. A. (1975). On the number of segregating sites in genetical models without
643 recombination. *Theoretical Population Biology*, 7(2), 256–276.
644 [https://doi.org/10.1016/0040-5809\(75\)90020-9](https://doi.org/10.1016/0040-5809(75)90020-9)
- 645
- 646

647 **Data availability statement**

648 Fastq sequence files, SFS and scripts are available from the Dryad Digital Repository:

649 <https://doi.org/10.5061/dryad.b8gtht7d1>.

650

651

652 **Authors contribution**

653 S.M. and P.L. conceived the project. S.P. provided reagents and samples. S.M. and P.L.

654 analysed the data and wrote the manuscript with input from S.P.

Tables

Table 1. Summary statistics and ABC estimation. Number of loci and SNPs after filtering, mean pairwise difference (θ_π), Watterson theta (θ_w), Tajima's D (TD), posterior probability of the most supported model and its parameters (median value and 95% credible interval in parentheses).

	N° Loci	N° SNP	θ_π	θ_w	TD	Model (probability) [†]	Nm	T_{COL} [‡]	N_{ANC}
<i>G. cuvier</i> [§] (N=8)	117976	25785	0.00057	0.00051	-0.03	NS (0.84)	-	-	-
<i>C. amblyrhynchos</i> (N=12)	69490	68355	0.00216	0.00229	-0.23*	SST (0.85)	11.5 (3.0-22.0)	20456 (12567-75649)	40961 (1315-49276)
<i>C. limbatus</i> (N=13)	60812	43449	0.00180	0.00166	0.43*	SST (0.55)	6.6 (1.5-15.4)	50198 (475-245440)	25521 (1913-52820)
<i>C. melanopterus</i> [¶] (N=8)	926	784	0.00040	0.00030	0.691*	SST (0.89)	1.8 (0.7-3.0)	91719 (5000-291341)	34607 (2760-95380)
						<i>Priors</i> ^a	U: 0.001 - 100	U: 1 - 300000	U: 100 - 100000.

* Tajima's D values are significant ($p < 0.001$).

[†] Most supported model and its posterior probability.

[‡] T_{COL} is expressed in generations.

[§] *G. cuvier* is best represented by the NS model: its demography is depicted through the *stairwayplot* algorithm (see discussion).

[¶] Data from Maisano Delser et al. (2019).

^a Uniform prior distribution. The prior distribution of Nm is the product of two uniforms (one for N and one for m).

Table 2. Coalescent simulations of 50,000 Rad-loci under SST model, with mutation rate fixed to 1.93×10^{-8} per site per generation and N_{ANC} fixed to 50,000. Mean pairwise difference (θ_π), Watterson theta (θ_w), Tajima's D (TD), and number of segregating sites (S) are averaged over 100 replicates.

<i>Nm</i>	<i>T_{COL}</i>	θ_π [‡]	θ_w [‡]	TD	S
1	5000	0.0013	0.0011	0.531	23599
	15000	0.0013	0.0012	0.405	24094
	50000	0.0017	0.0016	0.406	32201
	∞ [†]	0.0161	0.0139	0.669	283564
5	5000	0.0017	0.0016	0.361	32443
	15000	0.0019	0.0018	0.191	37712
	50000	0.0028	0.0028	0.035	56474
	∞	0.0177	0.0150	0.749	306786
10	5000	0.0019	0.0018	0.180	36561
	15000	0.0021	0.0022	-0.087	44380
	50000	0.0031	0.0034	-0.364	69436
	∞	0.0180	0.0158	0.585	321619
15	5000	0.0019	0.0019	0.048	38919
	15000	0.0022	0.0024	-0.274	48479
	50000	0.0032	0.0038	-0.608	77391
	∞	0.0181	0.0163	0.465	331816

[†] Equilibrium model obtained by simulating $T_{COL}=\infty$.

[‡] Theta values are expressed per site per generation.

Figure Legends

Figure 1. Evolutionary scenarios considered in this study (to both infer parameters in real data under an ABC framework and to perform coalescent simulations). SST (FIM) model is a simplified version of SST-CH (FIM-CH) in which connectivity Nm is constant after T_{COL} . Details on each parameter are presented in the main text.

Figure 2. Posterior distribution of the number of migrants per generation Nm (panel A) and of the colonisation time of the array of deme T_{COL} (panel B) estimated under the stepping stone model (SST) for *Carcharhinus amblyrhynchos* (red), *Carcharhinus limbatus* (green) and *Carcharhinus melanopterus* (blue).

Figure 3. Panel A: variation of the effective population size (N_e) through time and its 75% confidence interval estimated by the *stairwayplot*. Panel B: normalized SFS computed as in (Lapierre et al., 2017). *Carcharhinus amblyrhynchos* is represented in red, *Carcharhinus limbatus* in green, *Carcharhinus melanopterus* in blue, and *Galeocerdo cuvier* in purple.

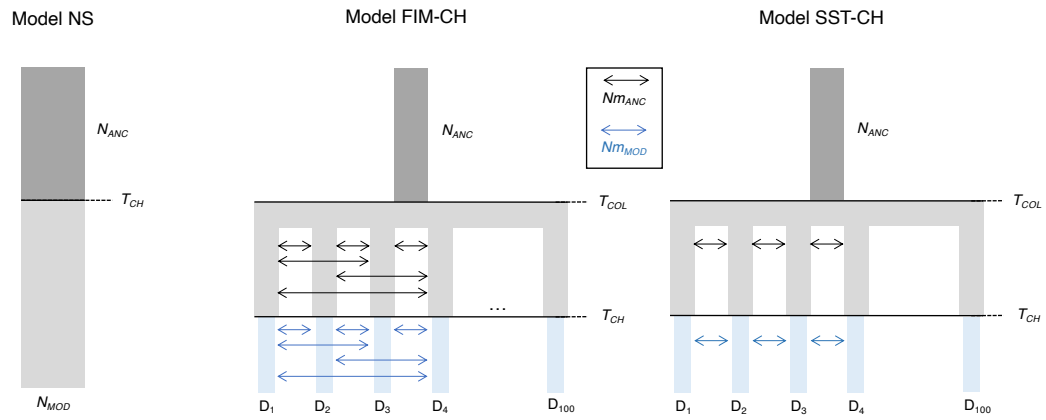
Figure 4. *stairwayplot* (maximum likelihood N_e and 75% confidence interval) (panel A) and normalized SFS (panel B) computed in simulated non-equilibrium SST scenarios with $Nm=1$, averaged over 100 replicates. Colonisation time of the array of deme T_{COL} occurred 5,000 (red), 15,000 (blue), and 50,000 (green) generations B.P., visually represented by the vertical dashed lines in panel A. The normalized SFS expected under a constant size non-structured model (NS constant size) is also shown (grey dashed line in panel B).

Figure 5. *stairwayplot* (maximum likelihood N_e and 75% confidence interval) (panel A) and normalized SFS (panel B) computed in simulated non-equilibrium SST scenarios with $Nm=10$, averaged over 100 replicates. Colonisation time of the array of deme T_{COL} occurred 5,000 (red), 15,000 (blue), and 50,000 (green) generations B.P., visually represented by the vertical dashed lines in panel A. The normalized SFS expected under a constant size non-structured model (NS constant size) is also shown (grey dashed line in panel B).

Figure 6. *stairwayplot* (maximum likelihood N_e) (panel A) and normalized SFS (panel B) computed in simulated non-equilibrium SST scenarios with $T_{COL}=15,000$ generations B.P. and an instantaneous decrease of the deme size (N_{DEME}) forward in time at $T_{CH}=10$ generations B.P. Colours represent the long-term connectivity values: $Nm=1$ (blue), $Nm=5$ (green), $Nm=10$ (red), $Nm=15$ (black). Line style represents the 10-fold (small dashes) or 100-fold (dots) reduction of N_{DEME} , or constant Nm (continuous line). The vertical grey dashed line in panel A represents the simulated colonisation time T_{COL} .

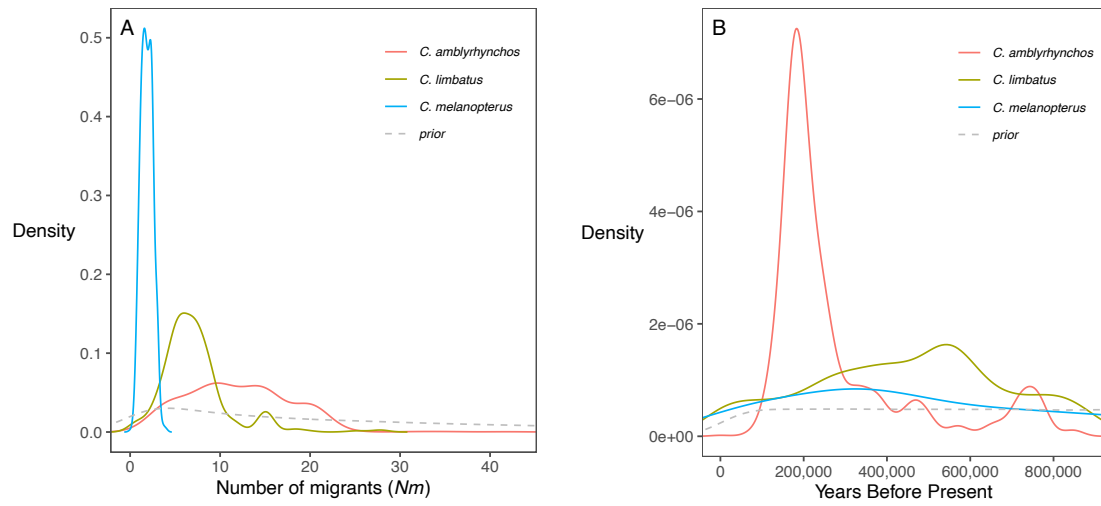
Figure 7. Schematic diagram representing the different coalescence phases in the history of lineages sampled from a deme belonging to a non-equilibrium meta-population. Each phase and related parameters are represented by a colour. Parameters influencing the coalescence rate in each phase are: the effective size of the deme (N_{DEME}) and the migration rate (m) for the *scattering* phase; the number of migrants exchanged per generation (Nm) and the number of demes (d) for the *collecting* phase; and the ancestral effective size (N_{ANC}) for the *ancestral* phase.

Figures



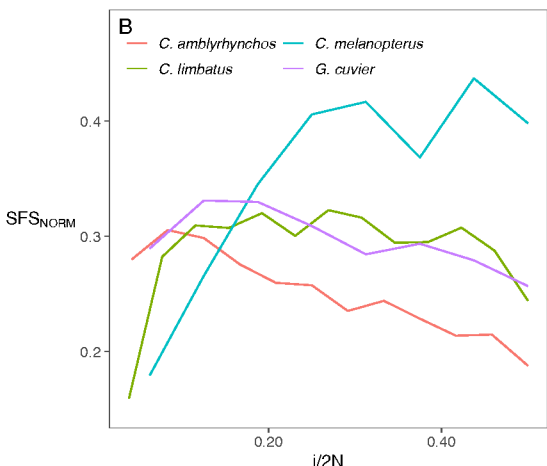
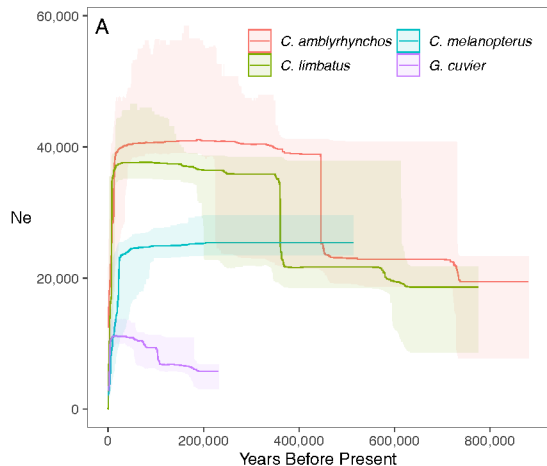
656

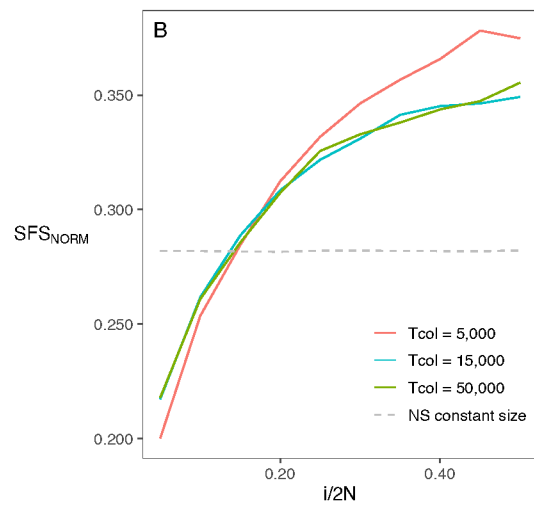
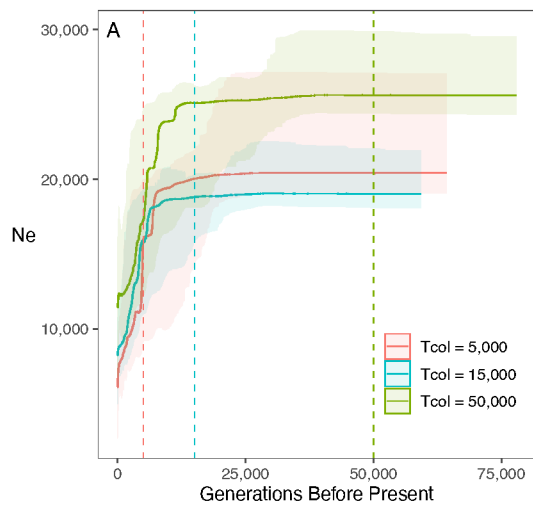
For Review Only

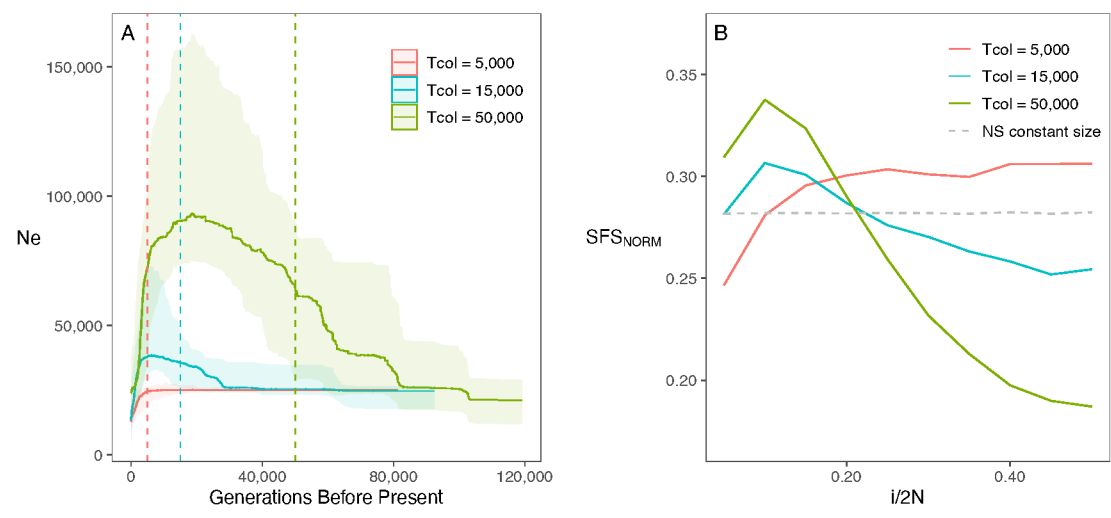


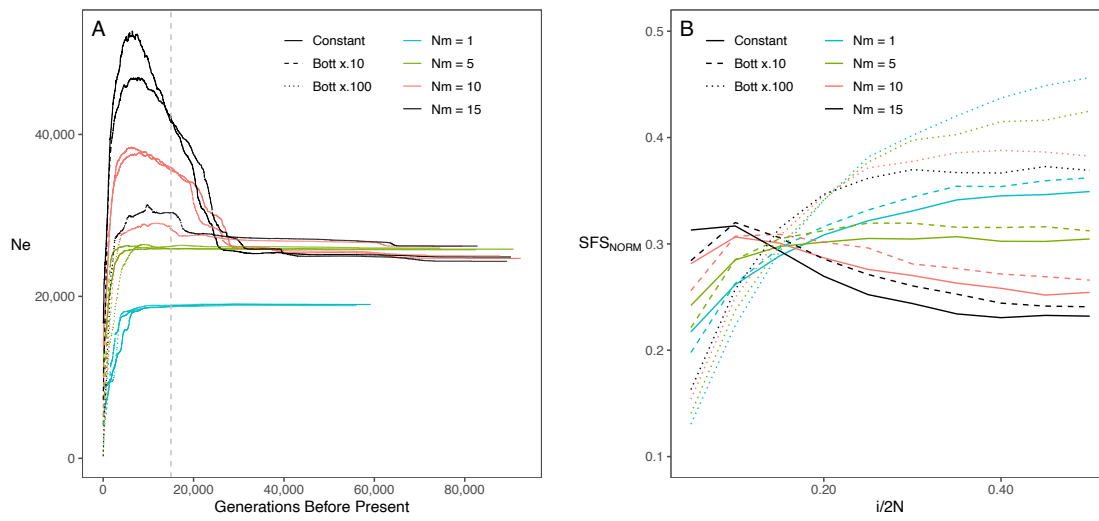
657

Review Only

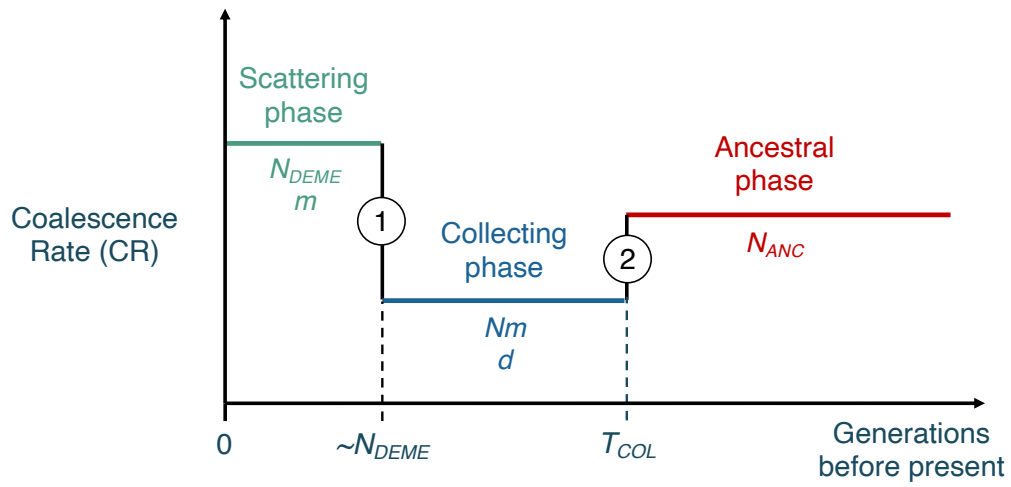








Jr Review Only



① $\Delta_{CR} < 0$: bottleneck

② $\Delta_{CR} > 0$: expansion

view Only